DFT Investigation of Electro-Optical Properties of a Novel Liquid Crystal Molecule Under Extraneous Electric Field (THz)

Yadupati Kushwaha[a], Satyabratt Pandey[b], Sachin Kumar Singh[b], Umesh Yadav[a]*

[a]*Department of Physics, DDU Gorakhpur University, Gorakhpur 273009, INDIA*
[b]*Department of Chemistry, DDU Gorakhpur University, Gorakhpur 273009, INDIA*

ARTICLE INFO

ABSTRACT

This work presents theoretical investigations into the electro-optical response of an aroylhydrazone liquid crystal (LC) N-[2-Hydroxy-4-dodecylidene]-N′-[4′-dodecyloxybenzoyl]hydrazine (2HDDH) under the influence of terahertz (THz) range electric fields, a regime rarely explored for this class of materials. While previous studies on LC molecules have predominantly focused on static or low-frequency fields, the effect of high-frequency (THz) electric fields on their electro-optical properties remains largely unexplored, limiting the understanding of their potential in next-generation photonic and optoelectronic technologies. Using a theoretical framework originally developed for organic compounds and extended here to THz device contexts, we computed order parameter, birefringence, director angle, vertical electronic transitions, frontier molecular orbitals (HOMO–LUMO), and molecular electrostatic potential (MEP) surfaces. The finite field approach was employed to evaluate order parameter, birefringence, and magic angle, while DFT and TD-DFT calculations revealed high anisotropic polarizability ($\Delta\alpha$ = 466.45 Bohr^3), a moderate dipole moment (μ = 5.67 D), and strong UV absorption. These results identify 2HDDH as a thermally stable, electro-optically active material with significant promise for THz-frequency optoelectronic applications, including advanced displays, sensors, and OLEDs.

1. Introduction

Besides the ordinary phases of matter, gas, liquid, and solid, a few substances exhibit other types of phases, which are in between the isotropic liquid phase and the most ordered solid phase. These mediatory phases are referred to as liquid crystal phases, and they possess orientational order as liquids and positional order as solids. Fluidity of such materials in liquid crystalline phases is like liquids, and anisotropic properties like solids [1-3]. Liquid crystal molecules have a unique structure that promotes the formation of supramolecules through self-assembling features of molecules. Calamatic LCs have a mesogenic rigid core formed by the connection of aromatic rings by linking groups and flexible side chains. The liquid crystalline character of liquid mesogens is influenced by various non-bonding interactions like ionic dipolar interactions, hydrogen bonding, and charge transfer [4-8]. These interactions have a key role in the diverse properties and relevance of liquid crystals, particularly in soft condensed materials, which are of great interest in fields ranging from electronics to biomedicine [9-10].

Aroylhydrazone liquid crystals (LCs), a notable class of LC-materials having (–C(O)-NH-N=CH-) core, have garnered considerable attention in optoelectronics due to their distinctive electro-optical properties [11,12]. The presence of a hydrazone functional group attached to an aromatic ring allows these materials to appear in diverse liquid crystalline phases, as well as nematic, smectic, and columnar phases. These are the critical phases for their use

---

in applications such as liquid crystal displays (LCDs), smart materials, and sensors [13,14]. Thus, the non-covalent interactions driving the mesogenic behavior of liquid crystals directly contribute to the functionality of materials like aroylhydrazone LCs in a variety of advanced technological applications. The ability of aroylhydrazone LCs to exhibit such mesomorphic behavior makes them ideal candidates for next-generation electronic devices. The mesophase formation and properties of aroylhydrazone LCs are influenced by a combination of subtle and intramolecular factors. Subtle factors, like molecular length, shape, and flexibility, play a key role in how the molecules align and pack together, which directly impacts their mesophase behavior. Additionally, intramolecular factors like hydrogen bonding, conjugation within the aromatic rings, and the overall symmetry of the molecules are crucial in determining the stability and electro-optical characteristics of these liquid crystals [15-17]. These factors contribute to the unique ability of aroylhydrazone LCs to interact with external electric fields, making them valuable for display technologies and sensing applications. Recognizing the importance of the functional properties and synthetic versatility of aroylhydrazone derivatives, our research group has begun to explore the structure-mesophase property relationship of these compounds [16].

The nature of the LC molecules may be polar or non-polar depending on their physical structure [18-20]. LC molecules may have more electric dipole moment, either along the long molecular axis or perpendicular to it. Comparatively high eternal dipole moments along long molecular axes fortify the dielectric anisotropy, and such kinds of LCs orient along the applied electric field. Molecules having a low dipole moment across the long molecular axis orient perpendicular to the applied electric field [21]. Calamatic Nematic mesogens are attentive to the external electric field and easily rotate their long molecular axis along the electric field. Calamatic mesogens have burly electron conjugation that is essential for display devices and other applications. Dielectric anisotropy is responsible for the reorientation of molecules in electric fields. The reorientation of LCs plays an important role in electro-optical devices. The orientational order parameter of LCs alters in the applied external electric field, and the director angle or magic angle reorients in an external field. The LC molecules collectively respond to the applied external field, which results in fluctuation of the director angle [22]. In this study, we have computed the order parameter, birefringence, and director angle in the presence of an electric field. We have constructed HOMO-LUMO to investigate electro-optical properties, and MEP, which is useful in interaction studies by predicting the reactive sites of a molecule [23].

Liquid crystals (LCs) often exhibit significant absorption, which requires extremely thin LC layers for experimental measurements. In the ultraviolet region, the required layer thickness can be as small as 0.1 microns. Even slight irregularities in layer thickness can impact spectroscopic characteristics, leading to a diminished overall response [24,25]. High dipole moment chromophores, known for their strong interactions, play a crucial role in forecasting spectral shifts in UV-Vis spectroscopy. Computational simulations of UV-Vis spectra are highly effective at achieving accurate predictions. To study UV-Vis spectra, we have used time-dependent density functional theory (TD-DFT), which is particularly reliable in providing precise results [26,27]. This method enables the calculation of energies linked to electronic transitions between ground and excited states. Accurate determination of excitation energies and corresponding dipole moments is essential for designing spectroscopic probes with desired optical features [28,29].

2. Methodology

In the present study, the B3LYP/6-31G** functional has been selected for ground-state geometry optimization and initial electronic property evaluations due to its well-established reliability for main group elements, cost-effectiveness, and widespread validation in literature for modeling organic molecules, including liquid crystals. However, B3LYP may not always offer the best accuracy for excited-state properties. Therefore, to enhance the reliability of excited-state predictions, we employed the M06-2X functional in combination with the 6-31G** basis set for the TD-DFT calculations.

2.1. Order Parameter, Birefringence, and Director Angle

The structure of N-[2-Hydroxy-4-dodecylidene]-N′-[4′-dodecyloxybenzoyl] hydrazine (2HDDH) molecule is optimized in the ground state (in vacuo) through the B3LYP/6-31G** technique. We have utilized Gaussian16 [30] software for optimization and Gauss View 6 [31] for visualization. We have used B3LYP/6-31G** functional for theoretical study due to its credibility for main group chemistry, and quantification of non-covalent interactions along molecular structure prediction [32-35]. After optimizing and checking for any imaginary frequency, we applied an electric field along the long molecular axis (X-axis) and perpendicular to it in the plane of the molecule (Y-axis) in a range of 0.0000 (a.u) to 0.150 at regular intervals of 0.002 (a.u). At the atomic level, electric field and frequency are related as 1 a.u = 5.14 × 10 [11] V/m = 6.5 × 10^{15} Hz [36]. In the presence of different applied electric fields, we have evaluated the molecular polarizability of 2HDDH molecules. In our consideration, polarizability along the X-axis (long molecular axis) is extraordinary molecular polarizability (α_e) while polarizability along the Y-axis is ordinary molecular polarizability (α_o). Order parameters, birefringence, and director angle are evaluated utilizing the finite field technique. The total energy of a molecular system in the presence of a homogeneous electric field in the light of a finite field approach can be given as:

$$E = E_o - \mu_i F_i - \frac{1}{2}\alpha_{ij}F_iF_j - \frac{1}{6}\beta_{ijk}F_iF_j \quad (1)$$

where E_o and E are the total energy of the molecule before and after the application of the electric field, respectively. μ, α, β, and F are equivalent to dipole moment, polarizability, first-order hyperpolarizability, and the component of the electric field, while subscripts i, j, and k indicate X, Y, and Z direction. By numerical differentiation

concerning the finite electric field, we have utilized the formula given in equations (2), (3), and (4) for order parameter, birefringence, and director angle, respectively [37-38].

Order parameter,

$$S = \frac{\Delta \tilde{\alpha}}{\Delta \alpha} = \frac{(\alpha_e - \alpha_o)}{(\alpha_e + \alpha_o)} \tag{2}$$

Birefringence,

$$\Delta n = \frac{(\alpha_e - \alpha_o)}{6.3631} \left[R^3 - \left(\frac{2\alpha_o + \alpha_e}{20.244} \right) \right]^{-1} \tag{3}$$

where R is the radius of the liquid crystal molecule.
Director angle,

$$\theta = \cos^{-1} \left[\frac{(2S + 1)}{3} \right] \tag{4}$$

2.2. HOMO-LUMO and MEP Study

A molecule of liquid crystal of N-[2-Hydroxy-4-dodecylidene]-N′-[4′-dodecyloxybenzoyl] hydrazine is optimized (Fig. 1) in the ground state using density functional theory in conjunction with the basis set 6-31G**. Further, HUMO-LUMO and MEP of the molecule are constructed. B3LYP/6-31G** technique ensures an accurate depiction of the electron density distribution and provides reliable insights into the molecule's electronic properties [27,39]. The molecular geometry was optimized before the ESP calculation to ensure structural accuracy and minimize artifacts.
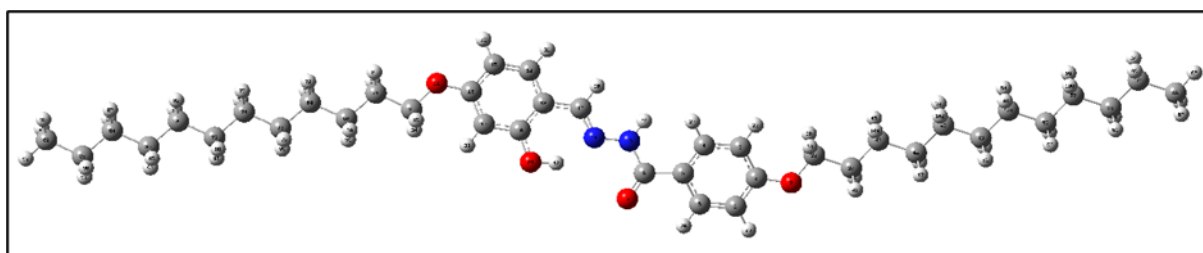

Fig. 1. Optimized molecular geometry of 2HDDH obtained using the B3LYP/6-31G** method, showing the spatial arrangement of functional groups and the extended alkyl chains.

2.3. Electro-Optical, electronic, and thermal Parameter study

The optimized structure of the molecule is utilized to evaluate electro-optical properties like mean polarizability, isotropic polarizability, dipole moment, and molar refractivity. Molecular orbital energies E_{HOMO} and E_{LUMO} have been utilized in the calculation of global parameters like electron affinity, ionization potential, electronegativity, electrophilicity index, and chemical hardness [40-43].

2.4. UV-Vis spectra study

To predict the UV-Vis absorption spectra, TD-DFT calculations were utilized. The M06-2X functional, known for its accuracy in describing excited-state properties, was employed in conjunction with the 6-31G** basis set. The resulting excitation energies and oscillator strengths were used to construct the absorption spectrum using OriginPro 2024.

3. Results and Discussion

We have applied the electric field in the range from 0.00 to 0.150 a.u. in steps of 0.002 a.u and investigated the order parameter, birefringence, and magic angle (director angle). The nature of variation of the order parameter, birefringence, and magic angle in the range 0.000 a.u to 0.092 a.u is different from the range 0.092 a.u to 0.150 a.u. At higher field strengths (particularly beyond 0.092 a.u = 4.7×10^9 V/m), the molecular response is expected to enter a nonlinear regime. This may lead to enhanced hyperpolarizability and significant deviation from linear behavior, especially in anisotropic polarizability. Such nonlinearities are important for applications involving intense THz fields, indicating the molecule's potential for third-order nonlinear optical (NLO) applications. Further computational and experimental work will be needed to quantify hyperpolarizability and confirm these predictions.

3.1. Order parameter

We applied an external electric field in the range of 0.000 to 0.150 a.u. and evaluated the order parameter using equation (1). As shown in Figure 2, the order parameter increases from 0 to a peak value of 0.61 between 0.000 and 0.022 a.u., indicating progressive alignment of LC molecules along the field direction. Between 0.022 and 0.092 a.u., the order parameter remains nearly saturated with minor fluctuations, suggesting a stable smectic A phase, where molecules are arranged in layers with their long axes roughly perpendicular to the layer planes and aligned with the field. However, beyond 0.092 a.u., a sharp decline in the order parameter is observed. This abrupt transition is attributed to the electric-field-induced disruption of the smectic A phase. At this critical field strength, the torque exerted by the field surpasses the cohesive intermolecular forces (van der Waals and dipole-dipole interactions) that maintain the layered structure. As a result, the molecular alignment becomes unstable, leading to the collapse of positional and orientational order. The liquid crystal begins to exhibit isotropic-like behavior, where molecules lose their directional alignment and the order parameter approaches zero. This phase disruption is consistent with prior findings where strong electric fields are known to induce phase transitions in LCs from ordered to disordered states [44]. At higher fields (beyond 0.100 a.u.), the induced torque can overcome stabilizing intermolecular interactions and cause

realignment perpendicular to the initial orientation or field direction, leading to a negative order parameter.

3.2. Birefringence

The variation of birefringence (Δn) with applied electric field is shown in Figure 3. At low fields (up to ~0.022 a.u.), Δn is minimal (≈0.01), reflecting the random orientation of molecules. As the field increases, molecular alignment improves, leading to a gradual rise in birefringence. Between ~0.022 a.u. and ~0.092 a.u., birefringence reaches a plateau around 0.025, signifying a stabilized smectic A phase with high optical anisotropy.

At~0.092 a.u., the birefringence starts to decrease abruptly, consistent with the drop in the order parameter. This marks the onset of field-induced disruption of the smectic phase, where the alignment and layer structure are compromised. As the field continues to increase, the optical anisotropy diminishes due to the breakdown of molecular order [45]. With a further increase in the electric field strength, the molecular orientation undergoes significant reorganization. This reorientation enhances the polarizability component perpendicular to the long molecular axis. As a result, the difference between the refractive indices along and perpendicular to the field direction ($\Delta n = n_{\parallel} - n_{\perp}$) becomes negative, leading to negative birefringence. The observed transition from positive to negative birefringence with increasing field strength reflects a gradual shift in the dominant direction of electronic polarization, suggesting a molecular realignment away from the initial field-induced orientation. This behavior is indicative of a field-induced destabilization of the ordered phase and is consistent with anisotropic polarizability responses in highly aligned liquid crystal systems.
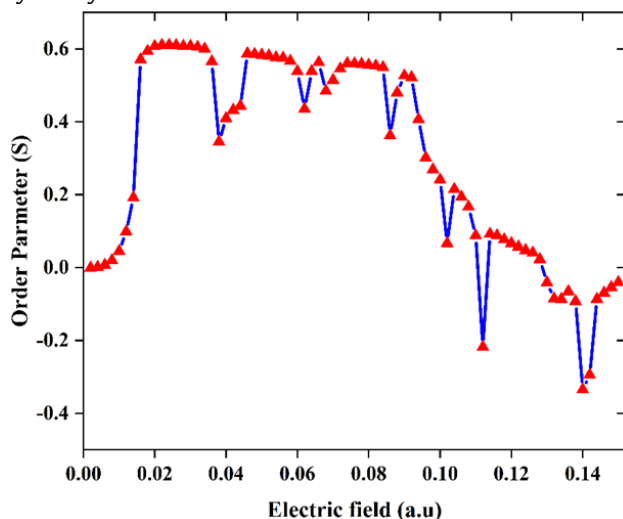

Fig. 2. Variation of order parameter with applied electric field using B3LYP/6-31G** method.

3.3. Director angle

The director angle is calculated with the help of mathematical equation 3 in the presence of the external electric field. The max and min values of the director angle are 83.6° and 42.2°, respectively (Fig. 4). When the applied electric field is very low, molecules are randomly orientated, and the average orientation of the molecule (director angle) from the applied electric field is about 70°.

As the electric field increases, the alignment of the smectic layer parallel to the electric field increases progressively; hence, the director angle decreases progressively with the increment of the applied electric field. In the Smectic A phase, its lowest value is 42.2°, and it slowly increases with the extension of the applied electric field up to 0.092 a.u. On further extension of the applied electric field director angle increases rapidly due to the collapse of positional and orientational order.
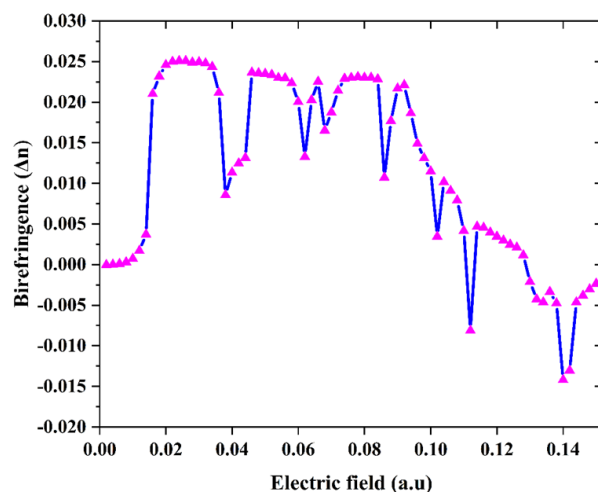

Fig. 3. Variation of birefringence with the electric field using B3LYP/6-31G** method.
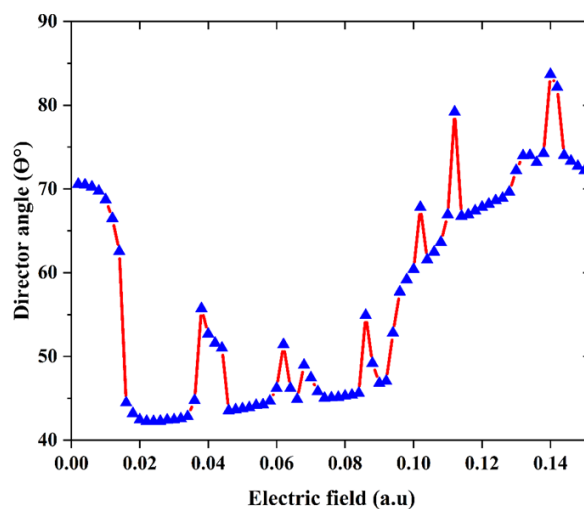

Fig. 4. Variation of director angle with applied electric field using B3LYP/6-31G** method.

3.4. HOMO-LUMO and Electrostatic Potential Surface

The HOMO and LUMO play a crucial role in determining the electro-optical behavior of the 2HDDH molecule. As shown in Figure 5, the HOMO is predominantly localized over the electron-rich aromatic rings, while the LUMO is distributed over the electron-deficient regions, suggesting an efficient intramolecular charge transfer. The calculated HOMO-LUMO energy gap reflects a balance between molecular stability and electronic excitability. A moderate gap facilitates optical absorption in the near-UV region, consistent with the UV-Vis results, and supports efficient charge transport under an external electric field. This gap also influences the molecule's polarizability and switching behavior, which are key parameters for its potential use in optoelectronic and liquid crystal display (LCD) applications. The electrostatic potential (ESP) surface of

the liquid crystal molecule (Fig. 6) visualizes charge distribution, crucial for understanding intermolecular interactions, alignment, and self-assembly in liquid crystalline phases. Red regions (high electron density) arise from oxygen atoms, acting as hydrogen-bond acceptors or dipole–dipole sites. Blue regions (low electron density) near nitrogen indicate positive potential, serving as hydrogen-bond donors. Green–yellow zones represent intermediate potential, typically carbon-rich alkyl chains, which impart amphiphilicity, fluidity, and promote hydrophobic interactions for stable layered mesophases. Aromatic cores with polar substituents (red/blue) enable π–π stacking, dipole alignment, anisotropy, and enhance responsiveness to external fields, key for LCD applications.
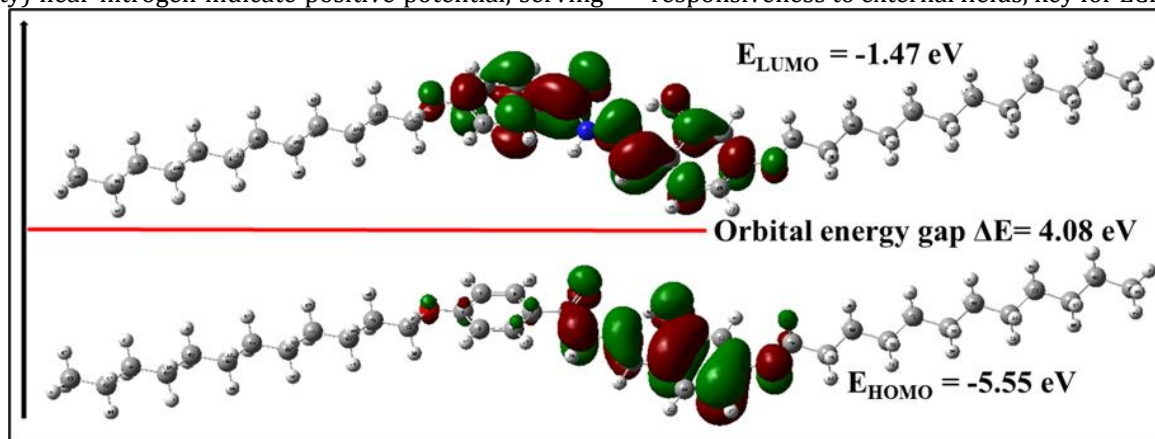

Fig. 5. Highest occupied molecular orbital (HOMO) and lowest unoccupied molecular orbital (LUMO) of 2HDDH obtained using the B3LYP/6-31G** method, illustrating the electron density distribution in the frontier molecular orbitals.
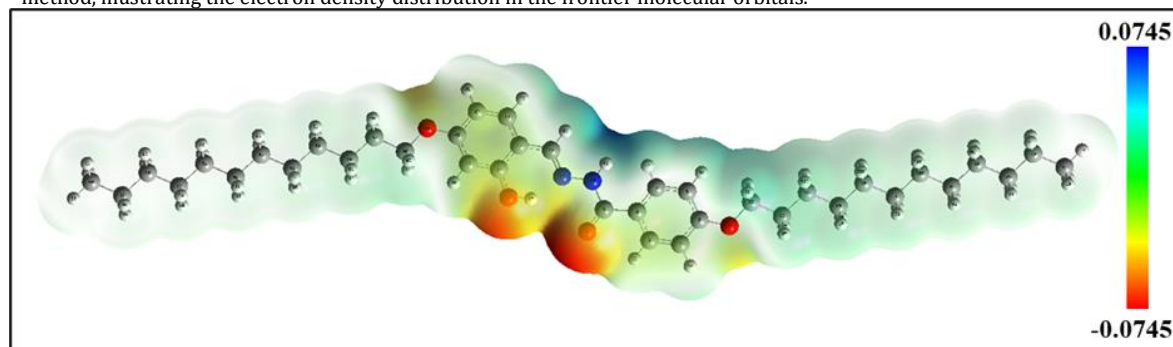

Fig. 6. MEP of the molecule anticipated at 0.004 electrons per bohr^3 isodensity surface using method B3LYP/6-31G**.

3.5. UV-Vis spectra Results: TD-DFT

The UV-Vis spectrum shows one intense and two weak electronic transitions. The most intense transition occurs at 295.04 nm (oscillator strength f = 1.0), attributed mainly to HOMO → LUMO (87.75%) and HOMO → LUMO+1 (4.89%) excitations. A weak transition at 250.17 nm (f = 0.2) arises from multiple excitations, primarily HOMO–1 → LUMO (50.0%) and HOMO–6 → LUMO+3 (24.0%). Another negligible transition is observed at 257.17 nm (Fig. 7). The strong absorption at 295 nm, located in the near-UV region, aligns well with the operational range of UV-responsive liquid crystal displays and UV filters, which typically function around 280–400 nm. The high oscillator strength and molar absorptivity suggest potential for applications in optoelectronic devices such as OLEDs and UV-photodetectors, as well as photovoltaic and photoconductive materials. Furthermore, the molecule's absorption properties in the UV-B region (280–320 nm) make it a suitable candidate for optical coatings or sunscreen formulations [46].

3.6. Electro-optical and Thermal Parameters

Electro-optical and thermal parameters are listed in Table 1. High dipole moment and polarizability anisotropy (Table 1) are prerequisites for electro-optical devices, as they improve the ability of molecules to align under an external field.
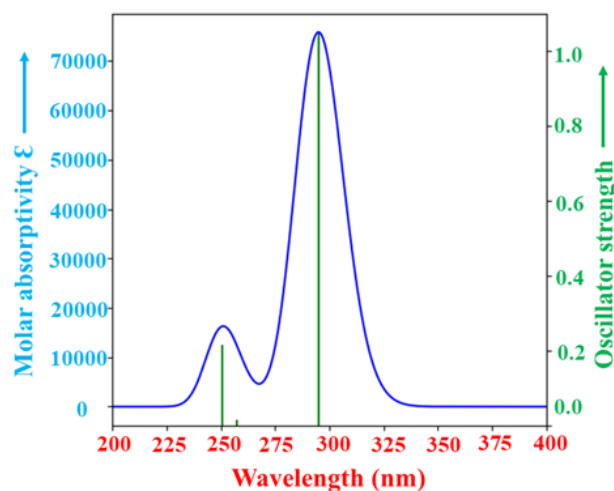

Fig. 7. Simulated absorption spectrum of 2HDDH calculated using the TD-DFT/M06-2X/6-31G** method, showing the electronic transition peaks and their corresponding wavelengths.

Highly anisotropic polarizability enhances optical switching frequency and contrast ratio. The liquid crystal

2HDDH has a moderate dipole moment (μ = 5.67 D) and a large anisotropic polarizability ($\Delta\alpha$ = 466.45 Bhor^3), suggesting it is a strong candidate for electro-optical applications. Moreover, the large Gibbs free energy (~514.84 kcal/mol) and enthalpy (320.36 cal/mol-K) values indicate robust thermal stability. Such stability ensures that the material can operate over a wide temperature range without structural or phase changes. This is essential for advanced displays and sensors, which may experience high operating temperatures or rapid thermal cycling [47]. A thermally stable liquid crystal will maintain its alignment and optical properties under these conditions, leading to consistent device performance and long operational lifetime. High ionization energy (I = 5.557 eV) and moderate electron affinity (A = 1.476 eV) suggest resistance to oxidation and some ability to accept electrons, indicating potential for interaction with electron-donating species. The balanced electrophilicity index (ω = 3.026 eV) and chemical hardness (η = 2.040 eV) imply a favorable mix of reactivity and stability; moderate hardness means the molecule can engage in intermolecular interactions (e.g., for nanoparticle doping) without compromising its integrity. Finally, the low electron-accepting capability (ω^+ = 1.526 eV) and high electron-donating capability (ω^- = 5.043 eV) make this material well suited for optoelectronic devices like OLEDs [48].

Table 1. Electro-optical, Thermal, and Global parameters of the 2HDDH molecule.

Electro-Optical & thermal parameters		Global Descriptors (eV)	
Dipole moment (μ)	5.67 Debye	Ionisation Potential (I)	5.557
Mean Polarizability (α)	526.88 (Bhor^3)	Electron affinity (A)	1.476
Anisotropic Polarizability ($\Delta\alpha$)	466.45 (Bhor^3)	Electronegativity(χ)	3.516
Molar refractivity	196.98 (esu)	Chemical hardness (η)	2.040
Enthalpy (H)	320.36 cal/mol-k	Chemical potential (φ)	-3.516
Gibbs free energy (G)	514.84 kcal/mol	Electrophilicity index (ω)	3.026
Zero-point energy	577.95 kcal/mol	Electron donating capability(ω^-)	5.043
Heat capacity (C_v)	184.02 cal/mol-k	Electron accepting capability(ω^+)	1.526

4. Conclusions

The theoretical investigations elucidate the potential of the compound 2HDDH for advanced optoelectronic applications. High anisotropic polarizability ($\Delta\alpha$ = 466.45 Bohr^3) and moderate dipole moment (μ = 5.67 D) of 2HDDH LC, making it suitable for electro-optical devices. Order parameter analysis and birefringence conform to its responsiveness in the external electric field. High Gibbs free energy and enthalpic value confirm its thermal stability. Global descriptors affirm the optical stability. The high value of electron-donating and moderate value of electron-accepting capabilities underlines its potential for OLED applications. The computational findings establish 2HDDH as a thermally stable and electro-optically responsive liquid crystal, promising for advanced applications in display technologies, sensors, and optoelectronic devices. Future work will investigate device integration and the bio-functional potential of the compound, aiming to advance next-generation materials for innovative technologies. Planned studies include quantifying hyperpolarizability under strong electric fields to evaluate suitability for third-order nonlinear optical applications. Additionally, device-level simulations and molecular docking will be employed to assess the compound's integration into optoelectronic devices and its potential in bio-functional applications such as biosensing and targeted delivery. It should be noted that this study is based exclusively on theoretical DFT calculations, which, while providing reliable predictions, are inherently subject to methodological approximations and the absence of direct experimental validation. Consequently, experimental studies are crucial to verify the predicted electro-optical properties and thermal stability of 2HDDH, as well as to evaluate its practical integration into optoelectronic and bio-functional devices.

Conflicts of interest

The authors declare that they have no known competing financial interests or personal relationships that could have appeared to influence the work reported in this paper.

Authors contribution statement

S.K.S. and U.Y. conceptualized this research work. S.B.P. and S.K.S. conceived the experiment. Y.K. and U.Y. performed theoretical calculations. Results have been discussed by all the authors. Y.K. drafted the manuscript, which was discussed, reviewed, and finalized by all the authors.

References

[1] De Gennes, P.G. and Prost, J., 1993. *The physics of liquid crystals* (No. 83). Oxford University Press.

[2] Klingbiel, R.T., Genova, D.J., Criswell, T.R. and Van Meter, J.P., 1974. Comparison of the dielectric behavior of several Schiff-base and phenyl benzoate liquid crystals. *Journal of the American Chemical Society*, *96*(25), pp.7651-7655.

[3] Mandal, P., Mitra, M., Bhattacharjee, K., Paul, R. and Paul, S., 1987. Nematic order of APAPA from X-ray diffraction and optical studies. *Molecular Crystals and Liquid Crystals*, *149*(1), pp.203-210.

[4] Korkmaz, B., Canli, N.Y., Özdemir, Z.G., Okutan, M., Gursel, Y.H., Sarac, A. and Şenkal, B.F., 2016. Synthesis and electrical properties of hydrogen-bonded liquid crystal polymer. *Journal of Molecular Liquids*, *219*, pp.1030-1035.

[5] Guan, L. and Zhao, Y., 2001. Self-assembled gels of liquid crystals: hydrogen-bonded aggregates formed in various liquid crystalline textures. *Journal of Materials Chemistry*, *11*(5), pp.1339-1344.

[6] Muthukumar, M., Ober, C.K. and Thomas, E.L., 1997. Competing interactions and levels of ordering in self-organizing polymeric materials. *Science*, *277*(5330), pp.1225-1232.

[7] Vikram, K., Singh, R.K. and Gupta, S.N., 2018. A new low-temperature solid modification in 1-isothiocyanato-4-(trans-4-propylcyclohexyl) benzene (3CHBT) probed by Raman spectroscopy and quantum chemical calculations. *Spectrochimica Acta Part A: Molecular and Biomolecular Spectroscopy*, *190*, pp.188-196.

[8] Vikram, K., Tarcea, N., Popp, J. and Singh, R.K., 2010. Temperature-dependent Raman study of the smectic to nematic phase transition and vibrational analysis using density functional theory of the liquid crystalline system 4-decyloxy benzoic acid. *Applied spectroscopy*, *64*(2), pp.187-194.

[9] Takanishi, Y., Takezoe, H., Watanabe, J., Takahashi, Y. and Iida, A., 2006. Intralayer molecular orientation in the B1 phase of a prototype bent-core molecule P-6-O-PIMB studied by X-ray microbeam diffraction. *Journal of Materials Chemistry*, *16*(9), pp.816-818.

[10] Achten, R., Cuypers, R., Giesbers, M., Koudijs, A., Marcelis, A.T. and Sudhölter, E.J., 2004. Asymmetric banana-shaped liquid crystals with two different terminal alkoxy chains. *Liquid crystals*, *31*(8), pp.1167-1174.

[11] Kagatikar, S. and Sunil, D., 2021. Schiff bases and their complexes in organic light-emitting diode application. *Journal of Electronic Materials*, *50*(12), pp.6708-6723.

[12] Mohan, M., Pangannaya, S., Satyanarayan, M.N. and Trivedi, D.R., 2018. Photophysical and electrochemical properties of organic molecules: Solvatochromic effect and DFT studies. *Optical Materials*, *77*, pp.211-220.

[13] Singh, H.K., Singh, S.K., Nandi, R., Rao, D.S., Prasad, S.K., Singh, R.K. and Singh, B., 2016. Observation of exceptional 'de Vries-like in a conventional aroylhydrazone based liquid crystal. *RSC Advances*, *6*(63), pp.57799-57802.

[14] Shanker, G., Prehm, M., Yelamaggad, C.V. and Tschierske, C., 2011. Benzylidenehydrazine-based room temperature columnar liquid crystals. *Journal of Materials Chemistry*, *21*(14), pp.5307-5311.

[15] Kanth, P., Rao, D.S., Prasad, S.K. and Singh, B., 2022. Investigation of mesomorphic, photophysical, and gelation behavior in aroylhydrazone-based liquid crystals: Observation of mesophase crossover phenomena. *Journal of Molecular Liquids*, *346*, pp.117084.

[16] Singh, S.K., Kumar, V., Nandi, R., Singh, H.K., Singh, R.K. and Singh, B., 2015. Microwave-assisted synthesis and mesomorphic investigations of p-substituted aroylhydrazones and their nickel (II) and copper (II) complexes. *Liquid Crystals*, *42*(2), pp.222-232.

[17] Singh, H.K., Pradhan, B., Singh, S.K., Nandi, R., Rao, D.S.S., Prasad, S.K., Achalkumar, A.S. and Singh, B., 2018. Substituted Aroylhydrazone Based Polycatenars: Tuning of Liquid Crystalline Self-Assembly. *Chemistry Select*, *3*(14), pp.4027-4037.

[18] Meyer, R.B., 1969. Piezoelectric effects in liquid crystals. *Physical Review Letters*, *22*(18), p.918.

[19] Balamurugan, S., Kannan, P., Yadupati, K. and Roy, A., 2011. Electro-optical switching studies on 1, 3-phenylene based banana shaped liquid crystals. *Journal of Molecular Structure*, *1001*(1-3), pp.118-124.

[20] Balamurugan, S., Kannan, P., Yadupati, K. and Roy, A., 2011. Electro-optical investigations and effect of asymmetry in bent-core liquid crystals. *Liquid Crystals*, *38*(9), pp.1199-1207.

[21] Sarna, R.K., Bhide, V.G. and Bahadur, B., 1982. Refractive indices, density and order parameter of some liquid crystals. *Molecular Crystals and Liquid Crystals*, *88*(1-4), pp.65-79.

[22] Ferrarini, A., Moro, G.J. and Nordio, P.L., 1996. Shape model for ordering properties of molecular dopants inducing chiral mesophases. *Molecular Physics*, *87*(2), pp.485-499.

[23] Kushwaha, Y., Singh, S.K. and Yadava, U., 2024. Insights into the electronic structure and interaction energies of 4-ethoxy-N-(4-ethoxy-2-hydroxybenzylidene) benzohydrazide. *Journal of Molecular Liquids*, *409*, p.125400.

[24] Tripathi, S., Ganguly, P., Haranath, D., Haase, W. and Biradar, A.M., 2013. Optical response of ferroelectric liquid crystals doped with metal nanoparticles. *Applied Physics Letters*, *102*(6).

[25] Jakeman, E. and Raynes, E.P., 1972. Electro-optic response times in liquid crystals. *Physics Letters A*, *39*(1), pp.69-70.

[26] Praveen, P.L., Ojha, D.P., 2012. Structure and electronic absorption spectra of nematogenic alkoxy cinnamic acids–a comparative study based on semiempirical and DFT methods. *Journal of Molecular Modeling* **18**, pp.1513–1521.

[27] Koch, W. and Holthausen, M.C., 2015. *A chemist's guide to density functional theory*. John Wiley & Sons.

[28] Song, Q., Gauza, S., Xianyu, H., Wu, S.T., Liao, Y.M., Chang, C.Y. and Hsu, C.S., 2010. High birefringence lateral difluoro phenyl tolane liquid crystals. *Liquid Crystals*, *37*(2), pp.139-147.

[29] Wu, Y., Zhou, Y., Yin, L., Zou, G. and Zhang, Q., 2013. Photoinduced liquid crystal blue phase by bent-shaped cis isomer of the azobenzene doped in chiral nematic liquid crystal. *Liquid Crystals*, *40*(6), pp.726-733.

[30] Frisch, M.J., Trucks, G.W., Schlegel, H.B., Scuseria, G.E., Robb, M.A., Cheeseman, J.R., Scalmani, G., Barone, V., Petersson, G.A., Nakatsuji, H. and Li, X., 2016. *Gaussian16 Revision A. 03 (Wallingford, CT: Gaussian Inc.)*

[31] GaussView, V.6.1, 2016, Roy Dennington, Todd A. *Keith, and John M. Millam, Semichem Inc, Shawnee Mission, KS*, *201*.

[32] Pandey, A. and Kumar, N., 2023. Tracing the transition from covalent to non-covalent functionalization of pyrene through C-, N-, and O-based ionic and radical substrates using quantum mechanical calculations. *RSC Advances*, *13*(21), pp.14119-14130.

[33] Yadava, U., Gupta, D.K. and Roychoudhury, M., 2010. Theoretical investigations on molecular structure and IR

frequencies of 4-n-nonyl-4′-cyanobiphenyl in light of experimental results. *Journal of Molecular Liquids*, *156*(2-3), pp.187-190.

[34] Kumar, N., Pal, B., Chaudhary, S., Singh, D. and Kumar, D., 2020. Reduced graphene oxide contains a minimum of six oxygen atoms for higher dipolar strength: A DFT study. *French-Ukrainian Journal of Chemistry*, *8*(1), pp.167-173.

[35] Antony, J. and Grimme, S., 2006. Density functional theory including dispersion corrections for intermolecular interactions in a large benchmark set of biologically relevant molecules. *Physical Chemistry Chemical Physics*, *8*(45), pp.5287-5293.

[36] Kumar, N., Singh, P., Chaudhary, S., Thapa, K.B., Upadhyay, P., Dwivedi, A.K. and Kumar, D., 2020. Spectroscopy Existing behind the Electro-Optical Properties with an Even-Odd Effect of nCB Liquid Crystal Molecules: A Theoretical Approach. *Acta Physica Polonica A*, *137*(6), pp.1135-1140.

[37] Kumar, N., Singh, P., Thapa, K.B. and Kumar, D., 2020. Molecular spectroscopy and adverse optical properties of N-(p-hexyloxy-benzylidene)–p-toluidine (HBT) liquid crystal molecule studied by DFT methodology. *IOP SciNotes*, *1*(1), p.015202.

[38] Kumar, N., Chaudhary, S., Singh, P., Thapa, K.B. and Kumar, D., 2020. Electro-optical odd-even effect of APAPA liquid crystal molecules studied under the influence of an extraneous electric field (THz): A theoretical approach. *Journal of Molecular Liquids*, *318*, p.114254.

[39] Parr, R.G., 1989. Density functional theory of atoms and molecules. In *Horizons of Quantum Chemistry: Proceedings of the Third International Congress of Quantum Chemistry Held at Kyoto, Japan, October 29-November 3, 1979* (pp. 5-15). Dordrecht: Springer Netherlands.

[40] Ridley, J. and Zerner, M., 1973. An intermediate neglect of differential overlap technique for spectroscopy: Pyrrole and the azines. *Theoretica chimica acta*, *32*(2), pp.111-134.

[41] Parr, R.G. and Pearson, R.G., 1983. Absolute hardness: a companion parameter to absolute electronegativity. *Journal of the American Chemical Society*, *105*(26), pp.7512-7516.

[42] Parr, R.G., Szentpály, L.V. and Liu, S., 1999. Electrophilicity index. *Journal of the American Chemical Society*, *121*(9), pp.1922-1924.

[43] Kushwaha, Y. and Yadava, U., 2025. DFT investigation on the effect of asymmetry on electro-optical properties of bent-core liquid crystals. *Phase Transitions*, *98*(1), pp.55-71.

[44] Helfrich, W., 1970. Effect of electric fields on the temperature of phase transitions of liquid crystals. *Physical Review Letters*, *24*(5), p.201.

[45] Raynes, P., 1993. LIQUID CRYSTALS — Second Edition, by S CHANDRASEKHAR, Cambridge University Press, (1992), ISBN 0-521-41747-3 (HB), ISBN 0-521-42741-X (PB). *Liquid Crystals Today*, 3(3), 7.

[46] Talukder, J.R., Lin, H.Y. and Wu, S.T., 2019. Photo-and electrical-responsive liquid crystal smart dimmer for augmented reality displays. *Optics Express*, *27*(13), pp.18169-18179.

[47] Collings, P.J. and Goodby, J.W., 2019. *Introduction to liquid crystals: chemistry and physics*. CRC Press.

[48] Parr, R.G., Gadre, S.R. and Bartolotti, L.J., 1979. Local density functional theory of atoms and molecules. *Proceedings of the National Academy of Sciences*, *76*(6), pp.2522-2526.